ERJ
Engineering Research Journal
Faculty of Engineering
Menoufia University

A THEORETICAL MODEL FOR PITTING PRODUCED BY CAVITATION

M.A. Hosien
Mechanical Power Engineering Department, Faculty of Engineering, Menoufyia University, Shebin El-Kom Egypt

ABSTRACT
The present paper is concerned with the mechanism of cavitation erosion. A theoretical model for the formation of a single pit produced by a microjet produced by a collapsing cavitation bubble is presented and the model developed to give the average surface slope of the eroded surface as a function of fluid velocity and cavitation number. The model predicts a threshold velocity below which no pitting can occur. A series of erosion experiments were conducted in water tunnel using pure aluminum plates positioned in the sidewall of the tunnel test section subjected to cavitating flow produced by various cavitating sources. The cavitating sources were 25 mm, 20 mm and 10 mm circular cylinder, 10 mm 60^0 symmetrical wedges, and 20 mm con.-div. wedge. The surface deformation produced on side wall specimens was analyzed by a surface finish measuring device. From the surface profiles, the surface slope and pit radius were computed. The experimental results were compared with the theoretical model and an encouraging agreement was found.

النموذج النظرى للحفر الناتج عن التكهف
هذه الدراسة متعلقة بالية التأكل الناتج عن التكهف. يعرض النموذج النظرى تشكيل حفرة واحدة ناتجة عن الارتطام الناتج عن انفجار فقاعة ناتجة عن التكهف وتم تطوير النموذج ليعطى متوسط الميل السطحى للسطح المتأكل كدالة فى سرعة السريان ومعامل التكهف. يتنبا النموذج بحد السرعة الذى اسفلة لا ينتج نقر.تم اجراء سلسلة من التجارب فى نفق مائى مستخدما شرائح الالومنيوم النقى التى وضعت فى جانب الجزء المعد من النفق والمعرض لحدوث التكهف بواسطة اشكال مختلفة كمصدر لحدوث التكهف. المصادر المختلفة للتكهف هى الاسطوانة الدائرية بابعاد 25,20,10 mm والمثلث المتماثل 10 mm و المثلث المتقارب المتباعد 20 mm. تم تحليل التشوة السطحى الناتج على الجدار الجانبى للعينة بواسطة جهاز قياس التشطيب السطحى. تم حساب بروفيل السطح وميل السطح ونصف قطر النقر. بمقارنة النتائج المعملية والنموذج النظرى وجد ان هناك توافق مرضى.

Keywords : Cavitation, Microjet, Erosion, Surface roughness, Cavitation number.

1. INTRODUCTION

Although the effects of cavitation have been observed long age, the actual mechanics of bubble collapse was not observed due to the high velocities involved. The mechanisms by which the erosion of a material occurs during cavity collapse are of fundamental importance to the study of cavitation erosion because the formulation of a theoretical treatment of cavitation erosion depends upon the damage mechanism.

Many investigations agree that cavitation erosion is the result of totally mechanical attack [1, 2 and 3]. The mechanical cavitation damage is due to the highly transient imposition of very intense and highly local forces on the surface. It is expected that there will be two types of damage produced by a cavitation bubble collapse; one is the effect of the shock wave radiated from the collapse center and the other is the microjet formed when the bubble collapses near a solid surface. Such a microjet is generated when the bubble collapse becomes substantially non-symmetrically. The materials subject to the impact of the shock wave or microjet undergo plastic deformation and become work hardened.

Until a few decades ago, the first mechanism which was proposed by Rayleigh [4], was accepted as the more realistic explanation for the erosion of materials. Rayleigh's analysis has been improved by several investigators. It was found that the pressure can reach extremely high values (10^2 - 10^4 MN/m^2 at an ambient pressure of 0.1 MN/rn^2 and with cavity gas pressure 10^{-4} MN/m^2). The shock wave intensity decreases inversely proportional to the radius from the center and close to this it would certainly be able to damage surfaces of solids.

Franc and Michel [5] estimated the impact pressures and the duration of this impact for four different phenomena associated with different forms of cavity collapse. They

distinguish impacts associated with the following phenomena: Micro bubble collapse, an impinging microjet, collective micro bubble cloud collapse and impacting cavitating vortices.

Peters et al. [6] predicted cavitation erosion using a numerical flow solver together with a new erosion model. The erosion model refers to the microjet hypothesis and uses information from the flow solution to assess the occurrence of microjet in specific areas. The ability of the numerical code to simulate cavitating flows was shown by comparison

with experimental tests of sheet cavitation over a NACA0009 hydrofoil. The numerical prediction of cavitation erosion was compared to measured erosion in experimental tests of an axisymmetric nozzle and shows good agreement regarding the erosive areas in general and the areas of highest erosion.

Kornfeld and Suvorov [7] suggested that liquid jets could be formed during cavity collapse. Eisenberg [8] speculated that jets formed during the asymmetrical collapse of cavitation bubbles could be responsible for the damage. These jets were experimentally shown by Naude and Ellis [9]. The occurrence of jet formation during collapse of single cavities was supported photographically by Kling and Hammitt [10], Lauterborn [11], Brunton [12] and Popoviciu [13]. The collapse of an initially spherical cavity near to a solid wall was determined theoretically by Plesset and Chapman [14]. The jet velocity was found to be 130 m/s at a collapse pressure of 0.1 MN/m^2. This implies an impact pressure up to 200 ME/m^2 when the jet strikes the sold wall. This impact pressure is sufficient to cause the observed cavitation damage in strong materials.

The work of Petkovšek and Dular [15] showed that no pits are produced during the formation of cavitation. In their experiment, the hydrodynamic cavitation evolution and cavitation induced erosion were synchronously recorded by two high-speed cameras. It was found the damage only occurs at cavitation cloud collapse.

Two main mechanisms are usually discussed: the microjet and pressure shock wave. For the case of the microjet it is believed that the liquid jet penetrates the bubble as the surrounding pressure is imbalanced. The jet velocity can reach a magnitude order of 100 m/s, and when it impacts the solid wall enormous stresses that cause pit formation occur [16]. Crum photographically presented the microjet phenomenon by a high-speed camera [17].

Many investigators showed that the damage was due to plastic deformation caused by the impact of microjets developed by the collapse of bubbles near to a solid surface [1, 18 and 19]. Vyas and Pceece [3] stated that the surface deformation of face centred cubic metals in a vibratory system is by shock waves and that the material removal is by ductile rupture from the lips of the craters. Shima [20] and Tsuda [21] reported that the damage was due to shock waves, microjets or both depending on the distance of the solid surface from the collapse centers. Rao et al. [22] and Eisenberg et al. [23] also are of the view that the damage may be due to either shock waves or microjets caused by the collapse of bubbles near solid surfaces. Knapp [24] and Thiruvengadam [25] support the shock wave mechanism concept.

Franc and Michel [26] estimated the impact pressures and the duration of this impact for four different phenomena associated with different forms of cavity collapse. They distinguish impacts associated with the following phenomena: Micro bubble collapse, an impinging microjet, collective microbubble cloud collapse and impacting cavitating vortices. The impact pressures and periods reviewed.

Dular et al. [27] suggested a model for the cavitation erosion process based on the damage caused when a bubble collapses in the vicinity of a solid surface. These single bubbles are supposed to be excited by the shock wave that is emitted from the collapse of a cavitation cloud. The cavitation erosion model is based on partly theoretical, partly empirical considerations, which are derived from knowledge that was gained during earlier studies of different authors. An obvious correlation between the cavitation structures and cavitation erosion was found through experimental investigations and statistical calculations.

In order to quantify the damage produced it is usual to postulate that a part of the energy stored by the cavitation bubble appears as energy dissipated in plastic work. Attempts have been made on this basis to correlate flow conditions and erosion rate [28, 29 and 30]. Generally, all these attempts suffer from the fundamental weakness that is very difficult to estimate accurately the amount of energy from cavitation bubble which lost by reflection from the surface and rebound of the collapse, i.e, the energy which never reaches the surface.

Therefore, the intent of this work is to establish a model for the formation of a single cavitation pit produced by an impinging of microjet which is formed during the collapse of cavitation bubbles. This model based on the idea of momentum transfer from the impact of microjet to the damaged surface.

2. PRODUCTION OF A CAVITATION PIT PRODUCED BY MICROJET

The general kinematic features of a microjet collision smooth, plane surface will be described on the basis of current analysis and experimental observations.

When ductile materials are subjected to impact by a microjet the deformation can be categorized as follows: 1. Elastic, 2. Elastic plus plastic, and 3. Hydrodynamic, i.e., viscous. For elastic deformation (category 1) there is no apparent damage after impact, whereas for category 2 a permanent deformation occurs. In category 3 the combination materials properties and impact conditions in such that solid responds as a viscous fluid. This occurs primarily in "hypersonic impacts" such as for example, collisions meteoroids and spacecraft. This type of collision is not concern for most other types of engineering applications.

Consider a pit produced by impact a single microjet from a collapsing cavitation bubble on the surface. The microjet impinging on surface is shown in Fig. 1. If the velocity of the microjet is u_j, then by momentum consideration and assuming that the velocities involved are much less than the speed of

sound, the pressure P produced in both liquid surrounding the microjet and solid surface subjected to the microjet is given by:

$$p = \rho c(u_j - u) \quad (1)$$

Where u: is the common velocity of the liquid and solid surface after the impact. ρ
and c are the density and speed of sound of the liquid respectively. When the material is subjected to impact by a microjet, the material responds elastically.
Then the relation between the pressure and velocity of solid is given by:

$$p = \rho_m c_m u \quad (2)$$

Where: ρ_m and c_m are the density and speed of sound of the solid material respectively. It assumed that the stress p_Y remains constant at the value required to produce the plastic flow of the material. Therefore, equation (1) is written as follows:

$$p_Y = \rho c(u_j - u) \quad (3)$$

Therefore, the velocity of deformation is given by:

$$u = u_j - (p_Y/\rho c) \quad (4)$$

The term $p_Y/\rho c$ is the critical velocity of the microjet (u_{jo}) necessary to produce plastic flow and at velocities below this value elastic strain can occur.

At the moment of microjet impinging on the solid surface two waves are radiated, one in the solid travels at the speed c_m and the other in the liquid travels at speed c as shown in Fig.1.

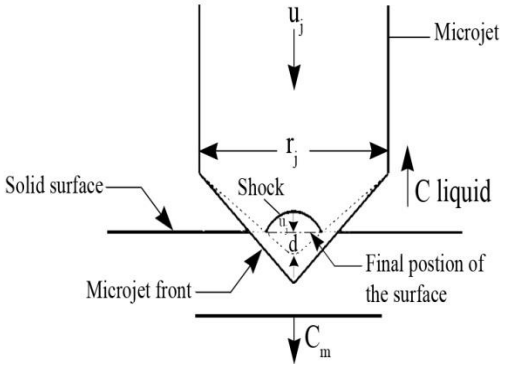

Fig.1. Sketch of microjet impinging on solid surface.

The plastic flow of solid surface occurs when the pressure waves have passed. Prior to this the pressure is given by equation (1) and (2) and consequently will be equal to the water hammer pressure of order $\rho c u_j$.
The plastic flow ceases when the pressure release wave in the liquid passes and the pressure falls to, p_r, while the deformation proceeds at a rate given by equation (4). Where pr is the pressure inside the bubble at the bubble radius (r).
The maximum depth of penetration of the microjet through the solid is limited by the difference in time taken for the release waves in the liquid and the solid to reach the impact center. At a radius, r, from the impact center less than the radius of the microjet, r_j, the time available for plastic flow, t_p, is given by:

$$t_p = \{[(r_j - r)/c] - [(r_j - r)/c_m]\} \quad (5)$$

During the impact of the microjet the solid surface moves with a velocity u. Therefore, the depth d(r) at radius r is given by:

$$d(r) = ut_p \quad (6)$$

Substituting from equation (5) into (6), the depth d(r) is given by:

$$d(r) = \frac{u(r_j - r)}{c}\left(1 - \frac{c}{c_m}\right) \quad (7)$$

This equation shows that a conical pit of radius r_j and maximum depth, d, is expected to form. Therefore, the maximum depth, d, is given by:

$$d = \frac{ur_j}{c}\left(1 - \frac{c}{c_m}\right) \quad (8)$$

The maximum angle of slope (∇) of the pit surface relative to the undeformed surface will be approximately d / r_j. Therefore, maximum angle of slope, ∇ , is given by:

$$\nabla = \frac{d}{r_j} = \frac{u}{c}\left(1 - \frac{c}{c_m}\right) \quad (9)$$

Substituting equation (4) into (9) the maximum angle of slope is given by:

$$\nabla = \frac{d}{r_j} = \frac{u_j - \left(\frac{p_Y}{\rho c}\right)}{c}\left(1 - \frac{c}{c_m}\right) \quad (10)$$

In case of a stationary empty bubble contains no gases or water vapour , the bubble will collapse completely, producing infinite pressures, Rayleigh [4]. If the bubble contains a certain amount of gas, total collapse will not occur, and the bubble will contract to a certain minimum radius determined by the quantity P_{go}/P_∞ , where P_{go} is the gas pressure in the bubble at the initial instant of compression which occurs owing to the pressure P_∞. Therefore, the maximum pressure, P_{max}, in the liquid will depend on the minimum bubble radius and on the P_{ro}/P_∞.
Assuming the process of the gas contraction during bubble collapse to be adiabatic, the minimum radius attained by the bubble in contraction will equal:

$$R_{min} = R_o\left[1 + (\gamma - 1)\frac{P_\infty}{P_{ro}}\right]^{-\frac{1}{3(\gamma-1)}} \quad (11)$$

If $P_\infty >> P_{ro}$, the previous formula can be simplified:

$$R_{min} = R_o\left[(\gamma - 1)\frac{P_\infty}{P_{ro}}\right]^{-\frac{1}{3(\gamma-1)}} \quad (12)$$

For the case in which γ =4/3:

$$R_{min} = R_o/\left[1 + \frac{1}{3}\frac{P_\infty}{P_{ro}}\right] \quad (13)$$

When the bubble reaches its minimum radius R_{min}, the pressure in the liquid will be greatest on the bubble boundary where it equal the pressure of the gas within the bubble. The latter can be represented in terms of the initial gas pressure P_{go} and the change in radius,

$$P_{max} = P_{ro}(\gamma-1)^{\frac{\gamma}{\gamma-1}}\left(\frac{P_{ro}}{P_\infty}\right)^{\frac{-\gamma}{\gamma-1}} = P_\infty^{\left(\frac{\gamma}{\gamma-1}\right)}(\gamma-1)^{\frac{\gamma}{\gamma-1}}P_{ro}^{\frac{-1}{\gamma-1}} \quad (14)$$

Assume that the initial gas pressure in the bubble is independent of the rate at which the bubble develops, and is determined by the gas content of cavitation nuclei. Therefore, it is assumed that P_{ro} to be constant. Then letting =1.4, the maximum pressure is given as:

$$P_{max} = K_1 P_\infty^{3.5} \quad (15)$$

Where K_1 is dimensional proportionality coefficient.

The magnitude of the microjet velocity can be estimated from the pressure causing the collapse of the cavitation bubble. According to the calculations of Plesset and Chapman [14], the microjet velocity is given by:

$$u_j = 12.8\sqrt{\frac{P_{max}}{\rho}} \quad (16)$$

Substituting equation (15) into (16) gives:

$$u_j = K_2 P_\infty^{\frac{3.5}{2}} \quad (17)$$

The cavitation number, σ, appropriate to conditions in the throat of the cavitating source is given by:

$$\sigma = \frac{P_\infty - P_V}{\frac{1}{2}\rho U_\infty^2} \quad (18)$$

Where: P_∞ and U_∞ the pressure and velocity in the throat of the cavitating source.

Substituting equation (18) into (17) yields:

$$u_j = K_3(U_\infty^2\sigma + P_V)^{\frac{3.5}{2}} \quad (19)$$

Neglecting P_v in respect to the term $U_\infty^2\sigma$ equation (9) becomes:

$$u_j = K_3 U_\infty^{3.5}\sigma^{1.75} \quad (20)$$

Substituting, u_j, equation (20) into equation (10), the maximum angle of slope is given by:

$$\nabla = \frac{K_3 U_\infty^{3.5}\sigma^{1.75} - (P_Y/\rho c)}{c}\left(1 - \frac{c}{c_m}\right) \quad (21)$$

The critical microjet velocity $u_{jo} = P_Y/\rho c$ is given by:

$$u_{jo} = K_3\, U_{\infty o}^{3.5}\, \sigma^{1.75} \quad (22)$$

Where $U_{\infty o}$ is a threshold velocity below which no pitting can occur.

Substituting equation (22) into (21) gives:

$$\nabla = \frac{K_3\sigma^{1.75}}{c}(U_\infty^{3.5} - U_{\infty o}^{3.5})\left(1 - \frac{c}{c_m}\right) \quad (23)$$

The wave in the solid travels at the speed c_m which is many times greater than the sound speed in the liquid and plastic flow cannot occur at a particular point until it has passed. The speed of the sound in the solid (aluminum) is three to four times greater than the speed of the sound in the liquid (water).Substituting

c / c_m equals 4 in equation (23) , the maximum angle of slope is given by:

$$\nabla = \frac{d}{r_j} = K_4\sigma^{1.75}(U_\infty^{3.5} - U_{\infty o}^{3.5}) \quad (24)$$

∇ : is the average surface slope.

The radius of the pit, r, will be simply equal to the radius of the microjet, $r = r_j$, which according to Plesset and Chapman [14], is about 0.1 of the maximum radius of the cavitation bubble. It is expected that the maximum cavitation bubble radius to be independent of fluid velocity and a function of cavitation number alone. K_4 and $U_{\infty o}$ are constant can be estimated from relevant test results.

3. EXPERIENTAL APPARATUS

A series of erosion tests were conducted in a cavitation research water tunnel with a parallel sided working section 40 x 20 mm cross section at the Faculty of Engineering, Menoyfia University. Details of the design description of this tunnel can be found in [31].The tunnel was designed so that the flow rate and pressure in the working section could be varied independently. The flow rate through the test section could be controlled by a bypass valve and the pressure by a control valve connected to an external compressed air supply. The cavitation was produced by a 25 mm, 20 mm, and 10 mm diameter circular cylindrical body, 10 mm 60^0symmetrical-wedge and 20 mm con-div bodies fitted centrally into the working section of the cavitation tunnel as shown in Fig. 2 .The erosion was determined using a plate of material of size 40 x 140 mm and 6 mm thick mounted on a side wall of the working section. The material used was pure aluminum and this is chosen because it exhibits almost perfect plasticity and is very easily eroded. The specimens were prepared by polishing to give a fine finish on the whole surface of the specimen.

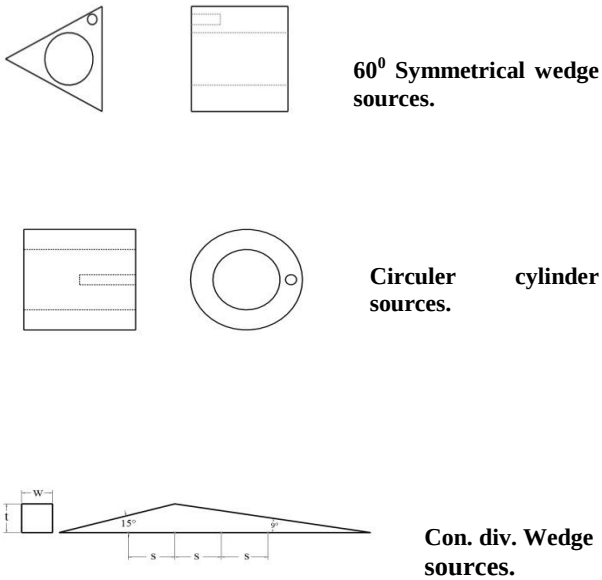

60^0 Symmetrical wedge sources.

Circuler cylinder sources.

Con. div. Wedge sources.

Fig. 2. Details of cavitating sources.

For the first series of the cavitation tests, the tunnel was run at a constant cavitation number, σ, appropriate to conditions in the throat .

$$\sigma = \frac{(P_\infty - P_v)}{\frac{1}{2}\rho U_\infty^2}$$

Where P_∞ and U_∞ are respectively the pressure and velocity in the throat. The value of σ chosen was 0.035 corresponding approximately to the maximum noise radiated from the collapse of the bubbles, and the throat velocity was varied over the range 24 to 40 m/s. The second series of tests consisted of running the tunnel at a constant velocity of 37 m/s and varying the cavitation number over the range 0.01 to 0.062.

The expected error in the cavitation number is about $\pm 6\%$. While the possible error in the flow velocity is about $\pm 1\%$.

4. MEASURMENT OF SURFACE DEFORMATION

The eroded specimens were analyzed using a FORSTER Profilograph Model 5815. The surface profiles were used to find the surface slope and the average pit radius. The scanning device used to measure the surface roughness has a diamond stylus with a rounded tip about 10 μm. The stylus speed and the operative length of traverse were kept the same for all the tests. This was accomplished by setting the speed of the stylus across the specimen surface equal to 0.5 m/s and the operative length of traverse equa1 to 8 mm.

The surface slope was obtained from the surface profiles. It was estimated by summing the modulus of the lateral movement of the stylus and dividing by the Length of the trace. On assuming that the average pit depth was twice the centerline average depth, the average pit radius was deduced by dividing the average pit depth by the previously calculated average surface slope. Further details of the method used to analyze the surface profiles are given in appendix 1.

The expected error in the surface slope is approximately $\pm 8\%$ and in the average pit radius is about $\pm 6\%$.

Photographs of some erosion specimens were taken using optical metallurgical microscope which is provided with a camera.

5. EXPERIMENTAL RESULTS AND DISCUSSION

All specimens exposed to cavitation have been studied by optical microscope. These investigations reveal that right from the beginning of cavitation exposure plastically deformed areas occur on the originally smooth surface. During the first part of the cavitation exposure the deformed areas are clearly separated indicating that each of them is caused by the collapse of a single cavity. If specimens are exposed to cavitation for different times but at a fixed cavitation condition, the maximum number of dents per mm^2 is expected to increase proportional to exposure time. This is verified by counting the number of dent in a small square (2 x2 mm) over the central area of the eroded specimen during the first part of the exposure time. The same trend was reported by Knapp [24], Hansson and Morch [32] and Lobo Guerrero [33]. At further cavitation exposure the dents are found to start overlapping, and a highly distorted surface develops with deformations of larger scale. The density of pits reaches a maximum when overlapping becomes significant and at further cavitation exposure the density of dents falls to a somewhat lower but constant level. This is shown in Fig.3 which covers exposure time up to 300 sec. The reason that the dents density reaches a maximum and then becomes constant is due to the interface of the damage areas and transformation of the overlapping dents into one large crater by a new cavity collapse in between them.

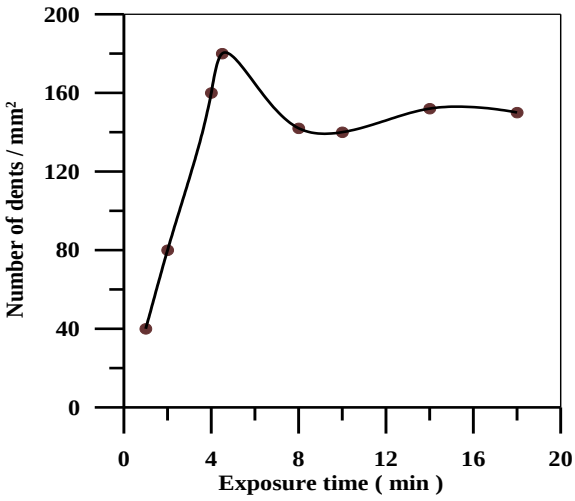

Fig. 3. Density of dents against cavitation time.

During the counting procedure the distribution of dent sizes on the specimen surface were measured for each dent. Fig. 4 shows the size distribution of the dents. This figure indicates that the percentage of dents of a given size always increases as the size under consideration is decreased, reaching a peak and thereafter decreasing. The range of dents sizes was found to be approximately 0.1—0.4 mm and over 50% of all dents were in the smallest sizes. Hammitt [2] has suggested that the diameter of typical microjets resulting from cavitation bubble collapse was in the range 1—80 μm, which is smaller than the dent size observed in the present experiments. The reason for this difference is that during the impact of the jet with the surface and during the formation of dent itself an outward flow of the liquid occurs

resulting in a dent size larger than the microjet diameter. However, the present experiments are not sufficient to give conclusive proof about the microjet size from the size of dents formed. Nevertheless, these values of dents sizes (0.1—0.4 mm) are compatible with the dent diameter observed with Knapp [24] using annealed aluminum. Dent diameters of 0.25 mm observed by Brunton [19] using thin metal foil.

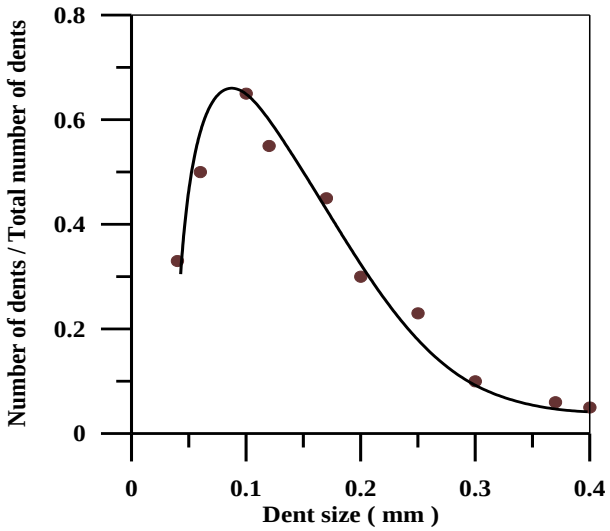

Fig. 4. Dents size distribution.

Fig. 5 shows a photograph of the specimen surface before being exposed to cavitation. Photographs and surface roughness measurements of deformed areas at different exposure times are shown in fig. 6. This is to allow a visual comparison to be made between the eroded end virgin surfaces. In general fig. 6 shows that the form of erosion pattern is deep dents in the central area of specimen. For this case, spherical collapse was unlikely because of the irregularity of the dents and the microjet mode is the cause of damage. Moreover, fig. 6 (surface measurements) indicates that the preformation of the bottom of dents is suggestive of jetting. This is because a shock wave in a depression would favor rounded hemispherical craters while repeated jetting leads to conical elongated pits as shown in Figure 6.

Smaller and shallower depressions appearing in large numbers are probable formed by microjets which are less intense than those necessary to form deep holes, if these are formed by a single cavitation event, Assuming that the damage is caused by microjets it is clear from the photographs and surface measurements that the collapse of cavitation bubbles results in a wide range of microjet intensities as described by their diameters

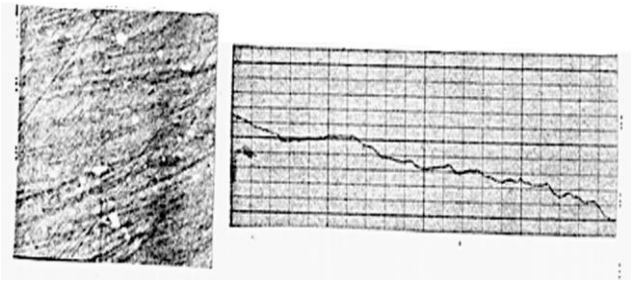

Fig. 5. Photograph and surface profile of aluminium before Exposure to cavitation.

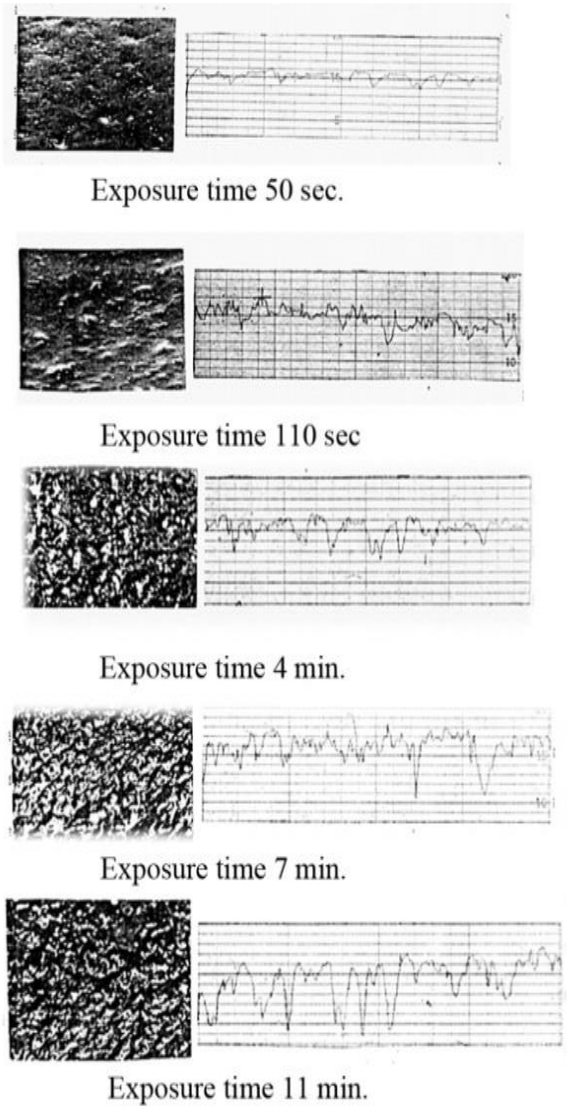

Fig.6. Photographes and surface roughness measurenments of aluminium after exposure to cavitation (x5).

From the surface profiles determined by FORSTER profilograph, the surface slope and the pit radius were calculated and plotted as function of exposure time. Fig. 7 shows the variation of surface slope with exposure time at various flow velocities ranged from 24 m/s to 40 m/s with a constant cavitation number of 0.035 for 10 mm 60^0 symmetrical wedge. In general fig. 7 indicates that the surface slope increases with time. It appears that the surface slope varies linearly with exposure time; the best fit straight lines to the data can be calculated using least squares are shown in fig. 7. It is reasonable to assume that the intercept of the straight line at zero time on the surface slope axis gives the level established very soon after the start of exposure, since the impact time is very small.

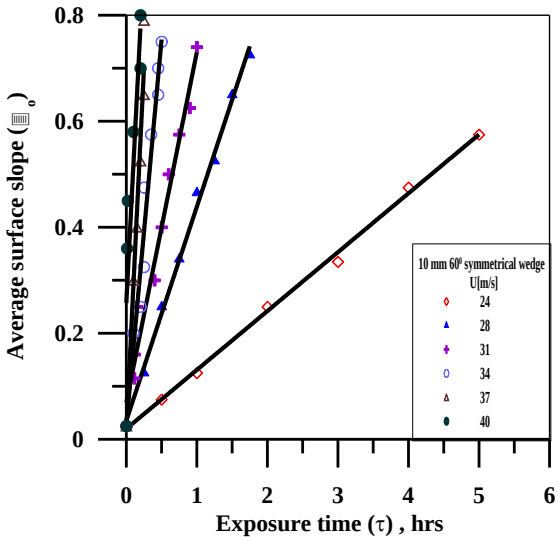

Fig.7. Typical average surface- slope- time curves at various throat velocities and constant cavitation number σ =0.035 for the 10 mm 60^0 symmetrical wedge with side wall specimens.

The variation of the surface slope at zero time from experiments with flow velocity at constant cavitation number for various cavitation sources is shown in figures 8 to 12. Also these figures show equation (24) applied to the experiments at a constant cavitation number of 0.035 with varying flow velocity. As shown in figures 8 to 11 a good correlation is in fact found between the measured and the calculated surface slope using equation (24).

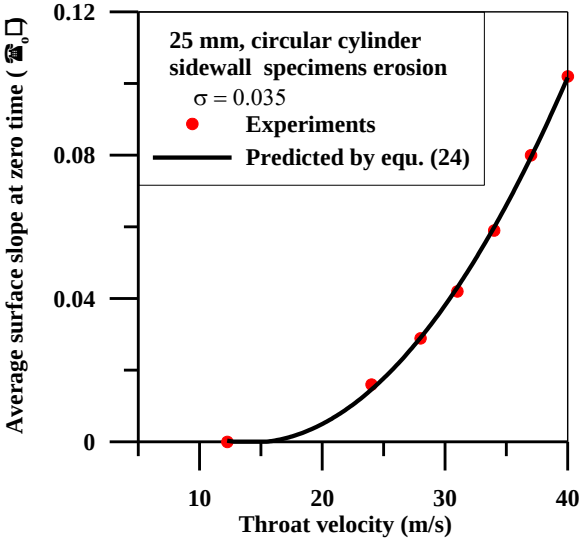

Fig. 8. Variation of average surface slope at zero time with throat velocity at constant cavitation number of σ = 0.035
for 25 mm circular cylinder.

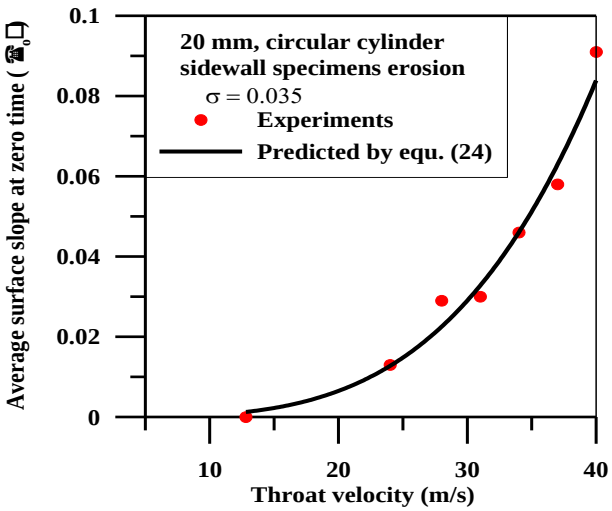

Fig. 9. Variation of average surface slope at zero time with throat velocity at constant cavitation number of σ = 0.035
for 20 mm circular cylinder.

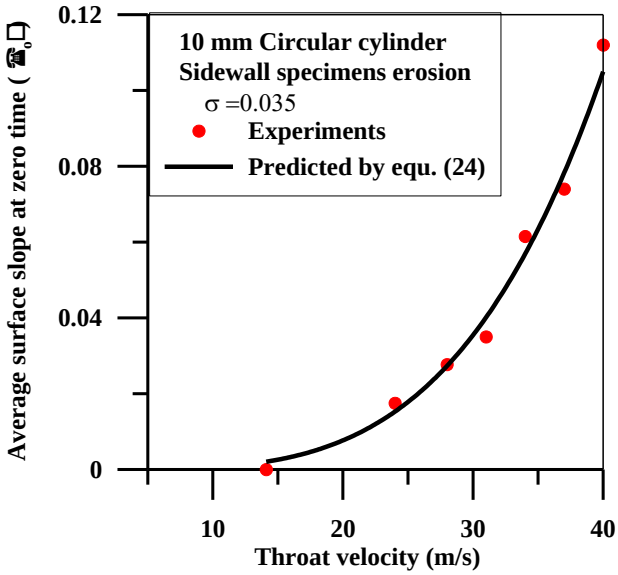

Fig.10. Variation of average surface slope at zero time with throat velocity at constant cavitation number of σ = 0.035 for 10 mm circular cylinder.

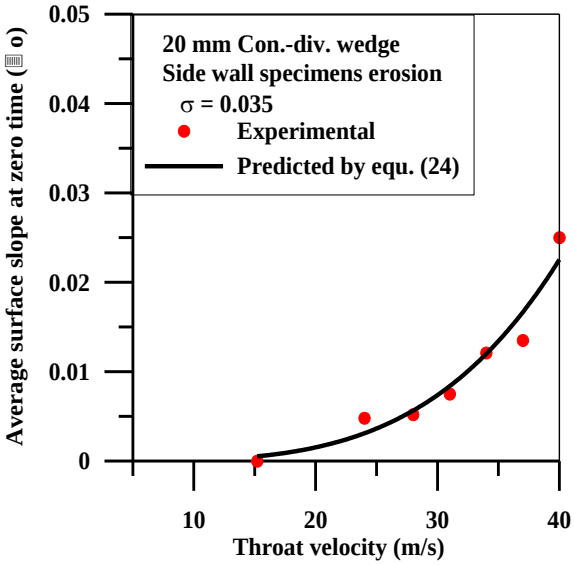

Fig.12. Variation of average surface slope at zero time with throat velocity at constant cavitation number of σ = 0.035 for 20 mm con.-div. wedge.

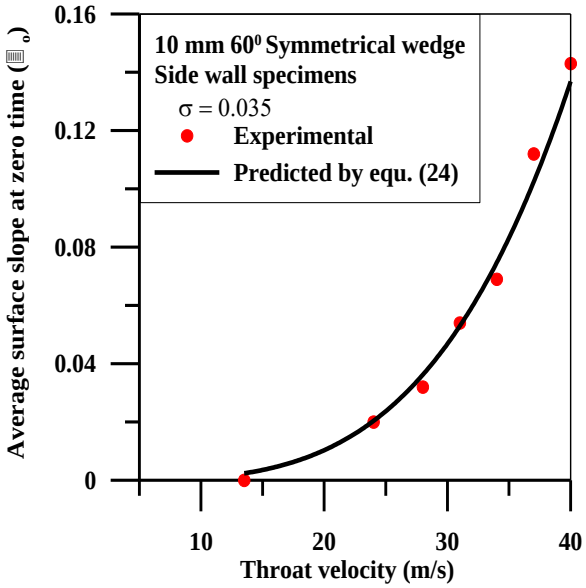

Fig. 11. Variation of average surface slope at zero time with throat velocity at constant cavitation number of σ = 0.035 for 10 mm 60^0 symmetrical wedge.

The constants k_4 and U_∞ in equation (24) were computed using the measured surface slope. It is clear that the threshold velocity below which no pitting on aluminum can occur is varied from 12.8 m/s to 15.2 m/s depending on the shape of cavitating source.

Figures 13 to 17 show the variation of the surface slope at zero time at constant flow velocity of 37 m/s with various cavitation numbers ranged from 0.01 to 0.062.

These figures show a similar trend to that shown in figures 8 to 12. In addition, these Figures illustrate that the average surface slope at zero time found by using the method of least squares increase with increasing the cavitation number at constant velocity. In addition, these figures indicate equation (24) applied to the experiments.

An encouraging agreement is found between the experimental results and the predicted results computed by equation (24).

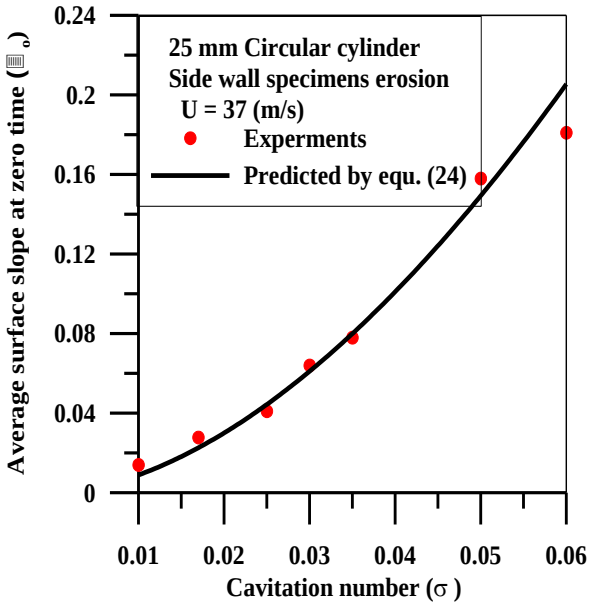

Fig.13. Variation of average surface slope at zero time with cavitation number at constant throat velocity of U_∞ =37 m/s for 25 mm circular cylinder.

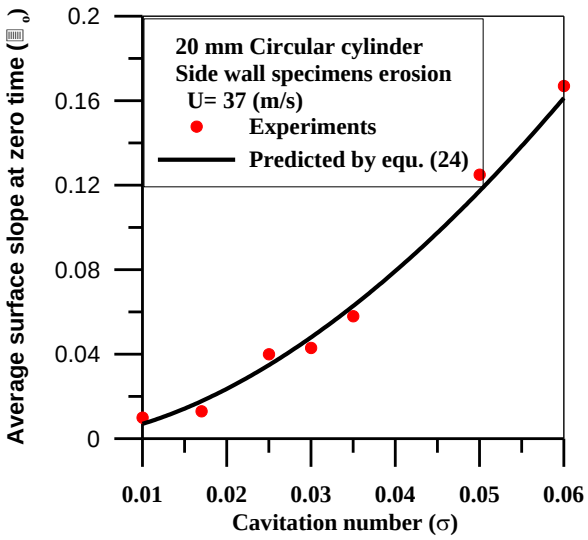

Fig.14. Variation of average surface slope at zero time with cavitation number at constant throat velocity of U_∞ = 37 m/s for 20 mm circular cylinder.

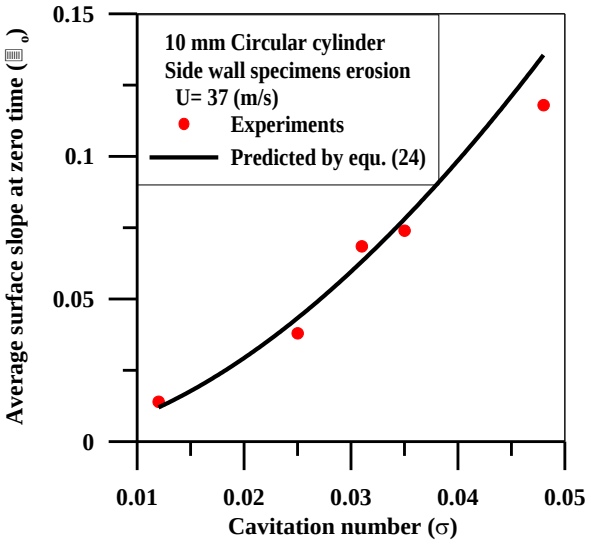

Fig.15. Variation of average surface slope at zero time with cavitation number at constant throat velocity of U_∞ = 37 m/s for 10 mm circular cylinder.

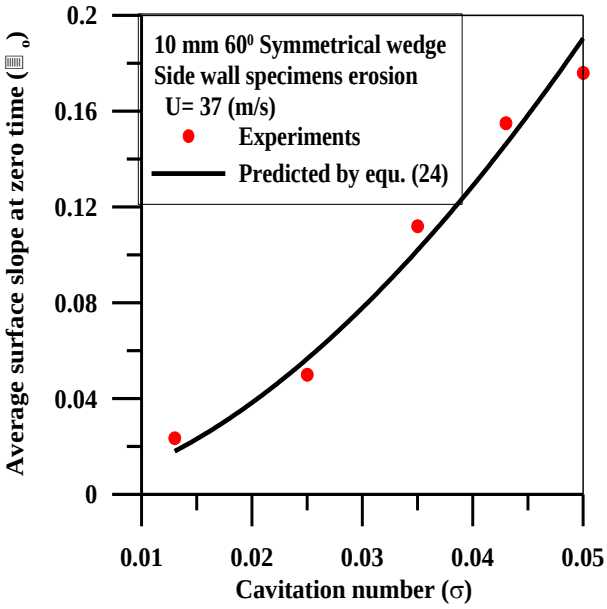

Fig.16. Variation of average surface slope at zero time with cavitation number at constant throat velocity of U_∞ = 37 m/s for 10 mm 60^0 symmetrical wedge.

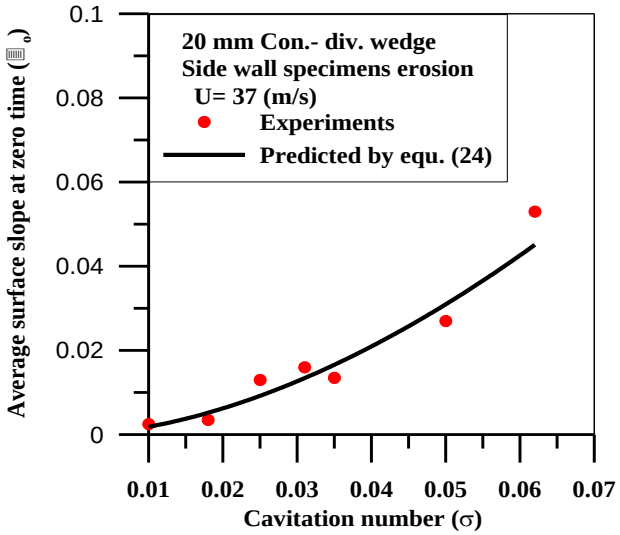

Fig.17. Variation of average surface slope at zero time with cavitation number at constant throat velocity of U_∞ = 37 m/s for 20 mm con.-div. wedge.

Fig. 18 shows the variation of the average pit radius with exposure time at various flow velocities. This figure indicates that the average pit radius may be independent of exposure time. Therefore, the mean values were determined and plotted as a function of flow velocity at constant cavitation number as shown in fig. 19. Fig. 19 indicates that the mean value of pit radius with flow velocity, showing a slight increase with flow velocity. A best fit line using least squares indicates that the slope is very small.
This agreement means that roles played by cavitation number are consistent with the present analysis.

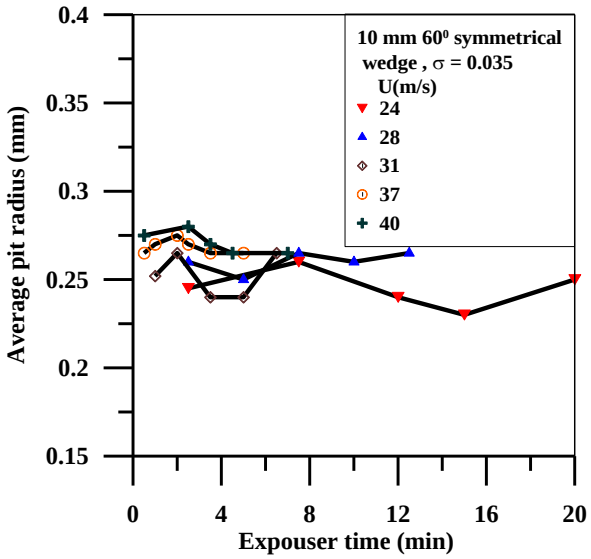

Fig. 18. Variation of average pit radius with expouser time at different velocities and σ = 0.035 for 10 mm 60^0 symmetrical wedge.

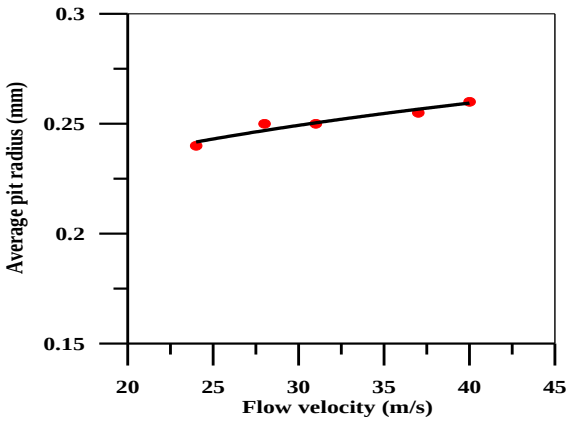

Fig. 19. Mean pit radius as a function of flow velocity with σ = 0,035 for 10 mm 60^0 symmetrical wedge.

Fig. 20 shows the variation of average pit with exposure tine at various cavitation numbers and constant flow velocity of 37 m/s. This figure shows considerable scatter in the data indicating that the average pit radius is probably independent of time. Fig. 21 is a plot of mean pit radius versus cavitation number. As shown in fig. 21, there is clearly a decrease in the mean pit radius with increasing cavitation number. The reason for this is that as the cavitation number increases the maximum bubble size decreases and therefore it appears that the mean value of pit radius may be proportional to the maximum bubble size. If it is assumed that the relationship between the mean pit radius and cavitation number is a power law, it can be shown by the method of least squares that the index which gives the best fit is 0.32 (i.e. $a \sim \sigma^{-0.32}$)

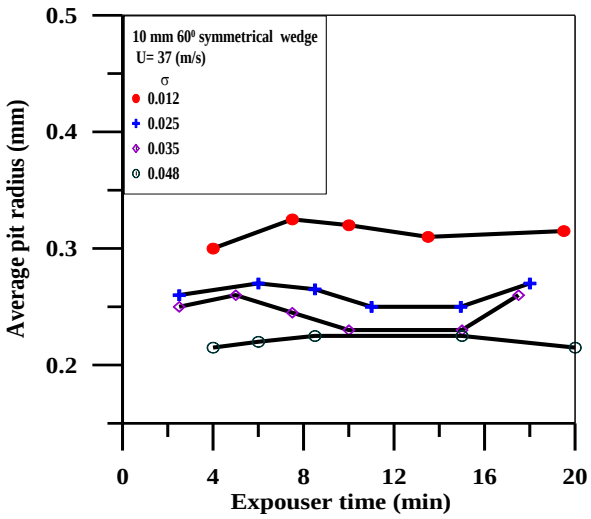

Fig. 20. Variation of average pit radius with expouser time at U_∞ =37 m/s and various cavitation number (σ) for 10 mm 60^0 symmetrical wedge.

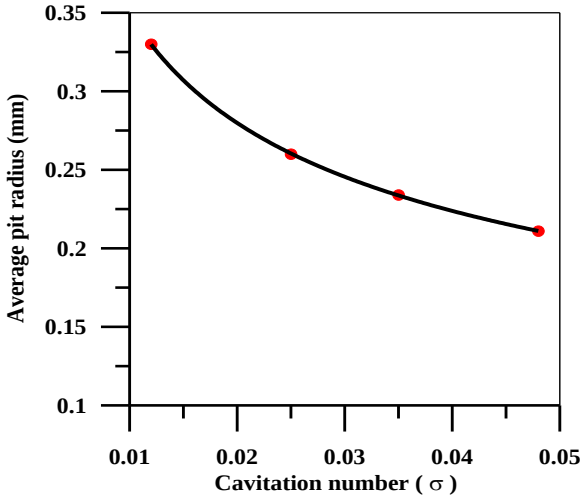

Fig. 21. Variation of average pit radius with cavitation number (σ) at U_∞ =37 m/s for 10 mm 60^0 symmetrical wedge.

6. CONCLUSIONS

The conclusions which can be drawn from these studies are:

1. The photographic evidence in this investigation does strongly indicate that, microjet are the dominant cause of pitting. In addition, no evidence of surface damage was found which could be linked directly with the spherical pressure wave mechanism.
2. A theoretical model has been developed to describe the formation of single pit produced by a microjet formed during collapsing of a cavitation bubble. The basic accomplishment of this initial effort has been to be able determine the average surface slope at zero time as a function of the cavitation number, and flow velocity and material properties. This effort will provide a firm foundation for the development of more complete model for the erosion mechanism in which the rate of weight loss can be predicted.
3. A critical flow velocities ranged from 12.8 m/s to 15.2 m/s below which not pit occur on pure Aluminum surface gives the best agreement with experiments.
4. The results indicate that the surface slope is dependent on the flow velocity and cavitation number as expected from the theoretical model. The pit radius is found to increase slightly with velocity but varies inversely as cavitation number. These results very similar and quite consistent with the observed cavitation.
5. A good encouraging agreement between the experiments results and theoretical analysis was observed.

REFERENCES

[1] Hammitt, F.G., (1969), "Collapse Bubble Damage to Solids," Cavitation state of knowledge, Ed. by Robertoson, J. and Wislicenus, G.F., ASME, New York, NY.

[2] Hammitt, F .G., (1980), "Cavitation and Multiphase Flow Phenomena", McGrew Hill, Int. Book Co., New Yorks.

[3] Vyas, B., and Pceece, C.M., (1977), "Cavitation of F.C.C. Metals", Metall Trans., V.8A, Jan.

[4] Rayleigh, L., (1917), "On the Pressure Developed in a Liquid during the Collapse of a Spherical Cavity", Published online: 08 Apr 2009. This article was downloaded by: [University of Sydney] On: 16 May 2013, At: 06: Philosophical Magazine Series 6, 34:200, 94-98.

[5] Franc, J.P., Michel, J.M., (2004),"Fundamentals of Cavitation", Kluwer Academic Publishers, Dordrecht.

[6] Peters, A., Sagar, H., Lantermann, U., and Moctar, O. E., (2015)"Numerical modelling and prediction of cavitation erosion", Wear, 338-339,189–201.

[7] Kornfield, M., and Suvorov, L., (1944),"On the Destructive Action of Cavitation", J. Applied Physics, Vol. 15, pp 495—506.

[8] Eisenberg, P., (1950),"On the Mechanism and Prevention of Cavitation", David Taylor Model Basin Report 712, Washington, D.C.

[9] Naude, C.F., and Ellis, T., (1961),"On Mechanism of Cavitation Damage by Non-Hemispherical cavities collapsing in contact with a Solid Boundary", Trans. ASME, J. Basic Engr., 83, D, 4.

[10] Kling, C.L., and Hammitt, F.G., (1972), "A photographic study of Spark Induced Cavitation Bubble Collapse", Trans. ASL, J. Basic Eng., 94, D,4.

[11] Lauterborn, W., (l979),"Liquid jet from Cavitation Bubble Collapse", Proc. 5th inter. Conf. on Erosion by Solid and Liquid Impact, Cambridge, England.

[12] Brunton, J.A., (1970), "Cavitation Damage", Proc. 3rd Int. Conf. on Rain Erosion, Royal Aircraft Establishment, Farnborough, U.K.

[13] Popoviciu, M., (1972), "A photographic Study of Spherical Bubbles Dynamics", Proc. of 4th Conf. on Fluid 1achinary, Budapest.

[14] Plesset, M.S., and Chapman, R.B., (1971),"Co11apse of an Initially Spherical Vapour Cavity in the Neighborhood of a So1d Boundary", J. Fluid Mech., Vol. 47, pp 283-290.

[15] Petkovšek, M., and Dular, M., (2013), "Simultaneous Observation of Cavitation Structures and Cavitation Erosion," Wear, 300(1), pp. 55–64.

[16] Franc, J. P., Riondet, M., Karimi, A., and Chahine, G. L., (2012), "Material and Velocity Effects on Cavitation Erosion Pitting", Wear, 274, pp. 248–259.

[17] Crum, L. A., (1995), "Comments on the Evolving Field of Sonochemistry by a Cavitation Physicist", Ultrason. Sonochem., 2(2), pp. 147–152.

[18] Robinson, M.J., and Hammitt, F.G., (1967), "Detailed Damage Characteristics in a Cavitating Venturi", Trans ASME, J. of Basic Engr., No.7 Ser. D, Vol.89.

[19] Brunton, J.H., Rochester, M.C., (1979),"Erosion of Solid Surfaces by the Impact of Liquid Drops", in Erosion, Ed., by C. M. Preece, Vol.,16, Academic Press, New York.

[20] Shima, A., Takayama, K., Tomita, Y., and Ohsawa, N., (1983),"Mechanism of Impact Pressure Generation from Spark - Generated Bubble Collapse Near a wall", A1AA Jr., Vol.21, No. l.

[21] Tsuda, Y., Uekl, H., Hirose, T., and Kimoto, H., (1982), "Experimental studies of shock Generation at the Collapse of Cavitation Bubble", Bulletin of JSME, Vol.25, No.210.

[22] Lakshmana Rao, N.S., and Symala Rao, B.C., (1977),"Prediction of Cavitation Erosion and the Role of Material Properties", Journal of the Institution of Eng. (India) Civil Eng. Div., V58.

[23] Eisenberg, P., (1970), "Cavitation and Impact Erosion –Concepts, Correlations, Controversies", ASTM, STP 474.

[24] Knapp, R.T., (1955),"Recent Investigations of Cavitation and Cavitation Damage", Trans, ASME, Vol.77.

[25] Thiruvengadam, A., (1967), "Theory of Erosion", Hydronautics Inc. Tech. Kept.

[26] Franc, J.P., and Michel, J.M., (2004), "Fundamentals of Cavitation", Kluwer Academic Publishers, Dordrecht.

[27] Dular, M., Sirok, B., and Stoffel, B.,(2006), "Experimental and numerical modeling of cavitation erosion", Sixth International Symposium on Cavitation, CAV2006, Wageningen.

[28] Kristensen, J.k., Hansson, I., and Morch, K. A., (1978),"A Simple Model for Cavitation Erosion of Metals", Journal of Physics D: Applied Physics, Vol.11.

[29] Kato, H., (1976),"On the Prediction Method of Cavitation Erosion from Model Test", IAHR Symposium on Two phase Flow and Cavitation in Power Generation Systems, Grenoble.

[30] Raabe, J. (1981),"Theoretical Approach of Erosion Rate Versus Speed and Cavity size on Wall-attached Cavitation", ASME Symposium on Cavitation Erosion in Fluid Systems, Boulder, Colorado.

[31] Hosien, M. A., and Selim, S. M., "A Study on Tip Clearance Vortex Cavitation Inception", Engineering Research Journal, Faculty of Engineering, Mataria-Cairo, Helwan University, Vol.122, June, 2009, M1-M25.

[32] Hansson, I., and Morch, K.A., (1978), "The Initial stage of Cavitation Erosion on Aluminium in Water Flow", Journal of Physics D: Applied Physics, Applied Physics, Vol. 11.

[33] Lobo Guerrero, J., (1974), "A Study of the Damage Capacity of Some Cavitating Flows", Ph. D. Thesis, Southampton University.

APPENDEX 1

Analysis of Surface Profiles

The erosion specimens were analyzed using a FORSTER profilograph Model 5815 to give the centerline average depth directly and to produce surface profiles, which were then used to find the average modulus surface slope (x/a) , this is defined by:

$x/a = \sum \Delta Y/l$

Where $\Delta Y$the ordinate is difference between adjacent turning points and l is the length of the sample. This definition can be expanded for ease of computation to give:

$x/a = 2/l\,(Y_1/2 - Y_2 + Y_3 - Y_4 + \cdots Y_n/2)$

Where the signs alternate regardless of the number of turning points considered (See Fig. A).

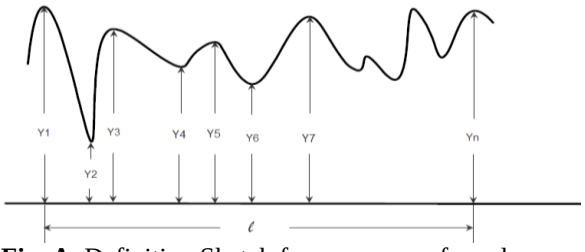

Fig. A. Definition Sketch for average surface slope.

Average Pit Radius

This can be defined as $a = l/(n-1)$

where n is the number of Y co-ordinates considered. It can be also calculated from average slope and average depth of pit as follows:

Average radius = Average Depth/Average slope

The average depth can be obtained from the following expression,

Average depth $= \sum \Delta Y/(n-1)$

The values of the average pit depth correlate well with the center line average recorded by the FORSTER Profilograph, being approximately equal to two times the center line average. Therefore, the average pit radius can be alternatively defined in terms of the center line average (CLA) as follows,

Average radius = 2CLA/Average slope